J Mater Sci: Mater Electron
DOI 10.1007/s10854-016-4482-9

Facile sonochemical preparation and magnetic properties of strontium hexaferrite ($SrFe_{12}O_{19}$) nanoparticles

P. Sivakumar[1] · Lior Shani[2] · Yosef Yeshurun[2] · Avner Shaulov[2] · Aharon Gedanken[1,3]

Received: 14 July 2015 / Accepted: 6 February 2016

Abstract The hard magnetic material M-type strontium hexaferrite ($SrFe_{12}O_{19}$) was prepared by a facile surfactant-free sonochemical strategy and subsequently by a calcination process. The surface morphologies, structures, and Curie temperature of the obtained final product was investigated by powder X-ray diffraction (XRD), high resolution scanning electron microscopy (HRSEM), transmission electron microscopy (TEM), BET (Brunauer–Emmett–Teller) specific surface area (SSA) and thermogravimetric analysis (TGA). XRD confirmed the formation of single-phase strontium hexaferrite with space group P63/mmc (194) and hexagonal structure and the mean primary crystallite size was found to be 44 nm. The morphology of synthesized $SrFe_{12}O_{19}$ product was in spherical shape with good crystalline nature. The measured Curie temperature (T_c) of the nanoparticles was around 462 °C. The magnetic property of the sample was measured by using a Superconducting Quantum Interference Device (SQUID) magnetometer at temperatures between 4 and 300 K. The measured saturation magnetization (M_s) at 300 K, 33 emu/g, is significantly lower than that found for bulk $SrFe_{12}O_{19}$, probably reflecting a size effect of the nano-particles.

✉ Aharon Gedanken
gedanken@mail.biu.ac.il

[1] Department of Chemistry, Bar-Ilan Institute of Nanotechnology and Advanced Materials, Bar-Ilan University, 52900 Ramat-Gan, Israel

[2] Department of Physics, Bar-Ilan Institute of Nanotechnology and Advanced Materials, Bar-Ilan University, 52900 Ramat-Gan, Israel

[3] Department of Materials Science & Engineering, National Cheng Kung University, 70101 Tainan, Taiwan

1 Introduction

Scientific and technological interest in magnetic ferrites has attracted attention to the hexagonal M-type hexaferrites $MFe_{12}O_{19}$ (M = Ba, Sr, or Pb) due to their relatively large saturation magnetization and high intrinsic coercivity [1]. These properties originate from the Fe^{3+} ions, which present high uniaxial magneto-crystalline anisotropy with single easy magnetization axis. The family of M-type hexaferrites is having an hexagonal magnetoplumbite crystal structure with space group P63/mmc and 64 atoms in unit cell, with a major axis, the *c*-axis, that defines the preferred magnetic direction in these permanent magnetic material. $SrFe_{12}O_{19}$ belongs to this family, and is a ferrimagnet in which iron ions in five different crystallographic sites are coupled antiferromagnetically. The most stable possible structure of $SrFe_{12}O_{19}$ with the lowest lattice energy contains Fe ions with anti-parallel spins which results in a net magnetic moment [2]. Its magnetic properties arise from interactions between metallic ions occupying particular positions relative to the oxygen ions in its hexagonal crystalline structure. Furthermore, the hexagonal strontium ferrite has 24 magnetic Fe^{3+} ions distributed among five crystallographically distinct magnetic sublattices, namely, three octahedral (2a, 12 k and $4f_2$), one tetrahedral ($4f_1$), and another one is a site in which ferric ion is surrounded by five oxygen atoms forming a trigonal bipyramide (2b). The magnetic moment and magnetocrystalline anisotropy of $SrFe_{12}O_{19}$ originate from the electronic structure of Fe^{3+} ions at the five distinct magnetic sublattices [2].

Strontium hexaferrite has found remarkable demand and challenging technological applications in fields such as telecommunications, magnetic recording media, magneto-optics, and microwave devices. This is due to the favorable

Published online: 12 February 2016

combination of sufficiently high magnetic properties, excellent chemical and physical stability, low production cost compared with rare-earth compounds, abundance of required raw materials, and relatively high Curie temperature, as well as low eddy current loss and high electrical resistivity [2]. The magnetic properties of the material depend mostly upon composition, distribution of substituted cations at five crystallographic sites, which is very much affected by its preparation method.

Therefore, many synthetic strategies have been applied with bottom-up approaches of preparation of $SrFe_{12}O_{19}$ to control particle shape, size, and magnetic properties. The synthetic techniques include citrate precursor technique [3], sol–gel method [4], co-precipitation method [5], microemulsion method [6], microwave-assisted combustion method [7], microwave-assisted calcination method [8], modified polyacrylamide gel method [9], sol–gel auto-combustion method [10–12], auto-combustion method [13], hydrothermal method [14, 15], solvothermal method [16, 17], electrospinning method [18], polymeric precursor method [19], molten-salt assisted coprecipitation method [20], glass–ceramic method [21], solid-state thermal decomposition method [22], solid-state reaction method [23], modified ceramic method [24], mechanochemical method [25], and ultrasonic spray pyrolysis method [26]. However, these methods suffer from high cost and a tedious synthetic procedure, which has urged to find new synthetic strategy to avoid this hurdle. Accordingly, to meet such requirements, a simple, inexpensive, environmentally compatibility, and scalable sonochemical synthesis approach has been investigated to obtain $SrFe_{12}O_{19}$ magnetic material to enhance the magnetic properties. Furthermore, the use of sonochemical irradiation during the homogeneous precipitation of the precursor solution is expected to shorten the precipitation time of the product along with a homogeneous distribution of the cations. Since, high intensive ultrasonic wave would lead to an acceleration effect in the rate of reaction and chemical dynamics, different properties of the final product such as purity, particle size, and shape can be controlled by changing the various synthetic parameters like sonication power, reaction temperature, and time [27].

The synthesis of nano materials by ultrasonic waves was carried out by many research groups. Nanomaterials such as metal oxides [28], alloys [29], coating [30] and nanocomposites [30, 31], and semiconductors [32] were prepared sonochemically. Sonochemistry uses ultrasound energy to induce chemical and physical changes in a medium through acoustic cavitation. In sonochemistry the chemical reactions occur at 20 kHz–1 MHz as a result of an implosive collapse of cavitation bubbles. This collapse creates very high temperatures and high pressures, conditions leading to the rupture of chemical bonds. Thus the continuous formation, growth, and implosive collapse of sonochemically generated bubbles leads to a local and extremely high increase in temperature (up to 5000 K), pressure (>200 MPa), and cooling rates (10^{10} K s^{-1}) in liquid [27]. In fact, our group has already reported on the synthesis of $SrFe_{12}O_{19}$ magnetic nanoparticles by the sonochemical technique and studied their properties. For example Sivakumar et al. [33] and I. Perelshtein et al. [34] have reported already on the synthesis of strontium hexaferrite fine nano powder through sonochemical technique using $Fe(CO)_5$ as a precursor. However, the precursor used in the present work is iron (III) acetylacetonate instead of the toxic $Fe(CO)_5$ used before. Moreover, the saturation magnetization of the final product is higher than that of the previous product [33].

In this paper, we report a facile and green sonochemical synthesis for the direct growth of $SrFe_{12}O_{19}$ followed by a simple calcination process for excellent magnetic properties. Structural, morphological, thermal, and magnetic characterization of the powder sample were carried out by powder X-ray diffraction (XRD), high resolution scanning electron microscopy (HRSEM), transmission electron microscopy (TEM), thermogravimetric analysis (TGA) under a permanent magnet, and Superconducting Quantum Interference Device (SQUID).

2 Materials and methods

2.1 Materials

All the chemicals were of analytical grade and used without any further purification. Strontium acetate ($(CH_3CO_2)_2Sr$) and Iron (III) acetylacetonate ($Fe(C_5H_7O_2)_3$; 97 %) were purchased from Sigma-Aldrich. Ammonia solution 30 % (NH_4OH) was purchased from Carlo Erba. The sonochemical synthesis process was carried out using a high-intensity ultrasonic horn (Ti horn, 20 kHz, 750 W at 50 % efficiency, Sonics & Materials Model).

2.2 Sonochemical preparation of $SrFe_{12}O_{19}$

In a typical synthesis procedure, Strontium acetate, 0.31 g (0.015 M), and Iron (III) acetylacetonate, 6.36 g (0.18 M) (the molar ratio of Sr^{2+}:Fe^{3+} was 1:12) were dissolved in 100 ml distilled water under magnetic string for 2 min to obtain a mixture, which was irradiated with high-intensity ultrasound radiation by employing a direct immersion horn. After 15 min 1 mL of NH_4OH solution was added drop by drop into the mixture to reach the pH value of around eight. The total time of ultrasound radiation was 1 h. Then the solution was dried on a hot plate at around 80 °C to evaporate the water. The solid was then dried in hot air at

100 °C for 5 h. Finally, $SrFe_{12}O_{19}$ powder was obtained by calcination in an ambient atmosphere at 1100 °C for 3 h at a ramping rate of 10 °C/min in a muffle furnace, followed by cooling to room temperature.

Figure 1 is a flow chart of the sonochemical synthesis of strontium hexaferrite ($SrFe_{12}O_{19}$) powder. The photographs of sonochemical apparatus from two different angles are shown in Fig. 2.

X-ray diffraction pattern of the sample was recorded on a Bruker D8 Advanced diffractometer using Cu K_α radiation (1.5406 Å) source. The diffraction data were collected over the 2θ range of 15–90° with an applied potential of 40 keV and current of 30 mA. Microstructural characteristics such as morphology, particle size, and crystal structure of the sample was analyzed by a high resolution scanning electron microscope (HRSEM) (HRSEM, FEI, Magellan 400 L, accelerating voltage 15 kV). TEM micrograph was obtained on a JEM-1400, JEOL transmission electron microscope with an accelerating voltage of 200 kV. Sample for the TEM study was prepared by dispersing and sonicating the powdered samples in isopropyl alcohol and adding a few drops of the resulting suspension to a TEM copper grid. BET (Brunauer–Emmett–Teller) specific surface area (SSA) was determined from nitrogen (N2) adsorption/desorption isotherms measured at liquid nitrogen temperature using a Nova 3200e Quantachrome analyzer. The specific surface area was calculated from the linear part of the BET plot. The Curie temperature (T_c) of the $SrFe_{12}O_{19}$ sample, heat treated at 1100 °C, was determined by thermogravimetric analysis (TGA) carried out on a TGA/SDTA851e device equipped with a small (10 Kgauss magnet) external permanent magnet, in the 25–800 °C temperature range, at a heating rate of 10 °C min^{-1} and under flowing nitrogen. In TGA analysis around 50 mg $SrFe_{12}O_{19}$ powder sample was used for studying Curie temperature (T_C). The magnetic properties of the $SrFe_{12}O_{19}$ nanoparticles were measured by a SQUID magnetometer (MPMS-XL5, Quantum design) at temperatures between 4 and 300 K. The powder was compressed, to avoid particles rotation.

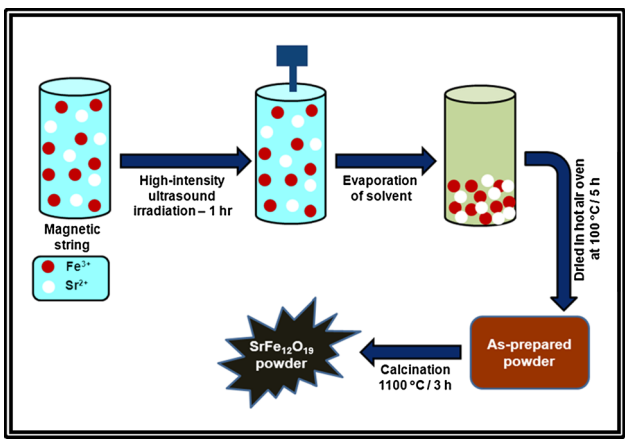

Fig. 1 Schematic illustration of synthesis process flow chart of $SrFe_{12}O_{19}$

3 Results and discussion

The phase purity and formation of M-type hexagonal $SrFe_{12}O_{19}$ was studied by powder X-ray diffraction measurement, which is the most valuable technique to identify the crystalline structure. Figure 3 shows the powder XRD pattern of the obtained $SrFe_{12}O_{19}$ powder. The indexed diffraction peaks in Fig. 3 are assigned to M-type of $SrFe_{12}O_{19}$ phase, which are in agreement with the standard JCPDF files (33–1340). The observed high intensity and sharp, well-defined peaks indicate that the high crystalline quality and most of the observed peaks correspond to the resulting product of $SrFe_{12}O_{19}$, with very small Fe_2O_3 (JCPDF: 33-0664) residual phase. All the diffraction peaks of the obtained product are consistent with those of the single phase, hexagonal structure and P63/mmc (194) space group. The crystallite size and lattice parameter for hexagonal ferrite structure was determined using:

$$D = \frac{0.9\lambda}{\beta \cos\theta} \tag{1}$$

$$\frac{1}{d^2} = \frac{4}{3}\left(\frac{h^2 + hk + k^2}{a^2}\right) + \frac{l^2}{c^2} \tag{2}$$

where 'D' is the average crystalline size, 'λ' is the wavelength of Cu K_α, 'β' is the full width at half maximum (FWHM) of the diffraction peaks, 'θ' is the Bragg's angle, 'a & c' are the lattice parameters, and 'hkl' the crystal plane index. The mean primary crystallite size (D) from the Scherrer's equation and lattice parameters (a, c) are calculated to be D = 44 nm, a = 0.5884 nm, and c = 2.3035 nm, respectively. The minimum value of standard deviation were Δa = 0.0002 nm and Δc = 0.0004 nm for the obtained $SrFe_{12}O_{19}$ powder. It shows that the obtained lattice parameter is trustworthy. Furthermore the all crystallographic planes have been used to calculate the lattice parameters of the prepared $SrFe_{12}O_{19}$ sample.

The morphology of the M-type strontium hexaferrite material has been examined by high resolution scanning electron microscopy (HRSEM) and transmission electron microcopy (TEM.). Figure 4 shows HRSEM and TEM images at different magnifications, histogram of particle size distribution, and EDX pattern analysis of the $SrFe_{12}O_{19}$ nanoparticles. The $SrFe_{12}O_{19}$ particles obtained show roughly spherical-like morphology and the average

Fig. 2 Photographs of sonochemical apparatus from two different angles

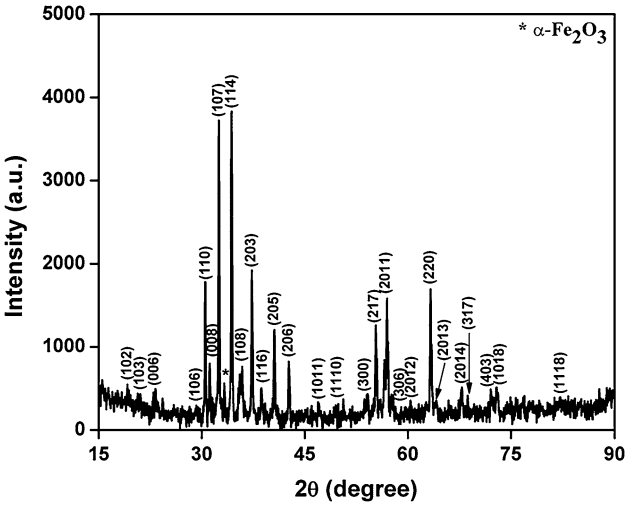

Fig. 3 Powder X-ray diffraction (XRD) pattern of $SrFe_{12}O_{19}$ powder by sonochemical process

particles size is 200 nm with little agglomeration. The low magnification HRSEM image (Fig. 4a) shows that the diameter of the nanoparticles ranges between 50–500 nm. It is suggested that any particle larger than 50 nm is an aggregate of smaller particles growing as a result of interparticle magnetic interactions.

The higher the synthesis temperature, the sharper are the edges of the obtained nanoparticles, suggesting a better crystallization of the obtained $SrFe_{12}O_{19}$ material. It is clear that the robust attractive forces among magnetic nanoparticles and higher the calcination temperature. Furthermore, from HRSEM and TEM images (Fig. 4b, d), at a high magnification, we can clearly observed that edge of the nanoparticles is sharp for the $SrFe_{12}O_{19}$ nanoparticles. Histogram of particles size and its distribution analysis of the $SrFe_{12}O_{19}$ nanoparticles obtained from HRSEM images are shown in Fig. 4e.

In order to prove the homogeneity of the sonochemically synthesized $SrFe_{12}O_{19}$ nanoparticles, energy dispersive X-ray spectroscopy (EDX) measurement test was carried out from HRSEM. The results display the presence Sr, Fe, and O elements in the EDX spectrum (Fig. 4f). The atomic ratio of strontium (Sr^{2+}) to iron (Fe^{3+}) detected from the EDX spectrum is approximately 1:12.

Furthermore, liquid nitrogen (N_2) adsorption and desorption isotherms were performed to characterize the specific surface area of the synthesized $SrFe_{12}O_{19}$ nanoparticles. The specific surface area was determined by using Brunauer-Emmett-Teller (BET) method, the calculated specific surface area of the prepared $SrFe_{12}O_{19}$ nanoparticles is 8.1 $m^2\ g^{-1}$.

Figure 5 displays the TGA curve of the $SrFe_{12}O_{19}$ nanoparticles under an external magnetic field. The Curie temperature of the sample, deduced from TGA measurements, (Fig. 5), is $T_c = 462$ °C. At this temperature a sharp drop in the mass (or force) is observed. This Curie temperature is somewhat higher than the value of 450 °C reported for bulk $SrFe_{12}O_{19}$ [35].

Figure 6 shows magnetic hysteresis loops for the $SrFe_{12}O_{19}$ nanoparticles measured by a SQUID magnetometer (MPMS-XL5, Quantum design) at 100 and 300 K. Evidently, the loops are somewhat distorted, exhibiting a narrow 'waist' at low external fields and a tendency to saturate at low as well as high fields. This is mostly pronounced at low temperatures. In Table 1 we summarize the

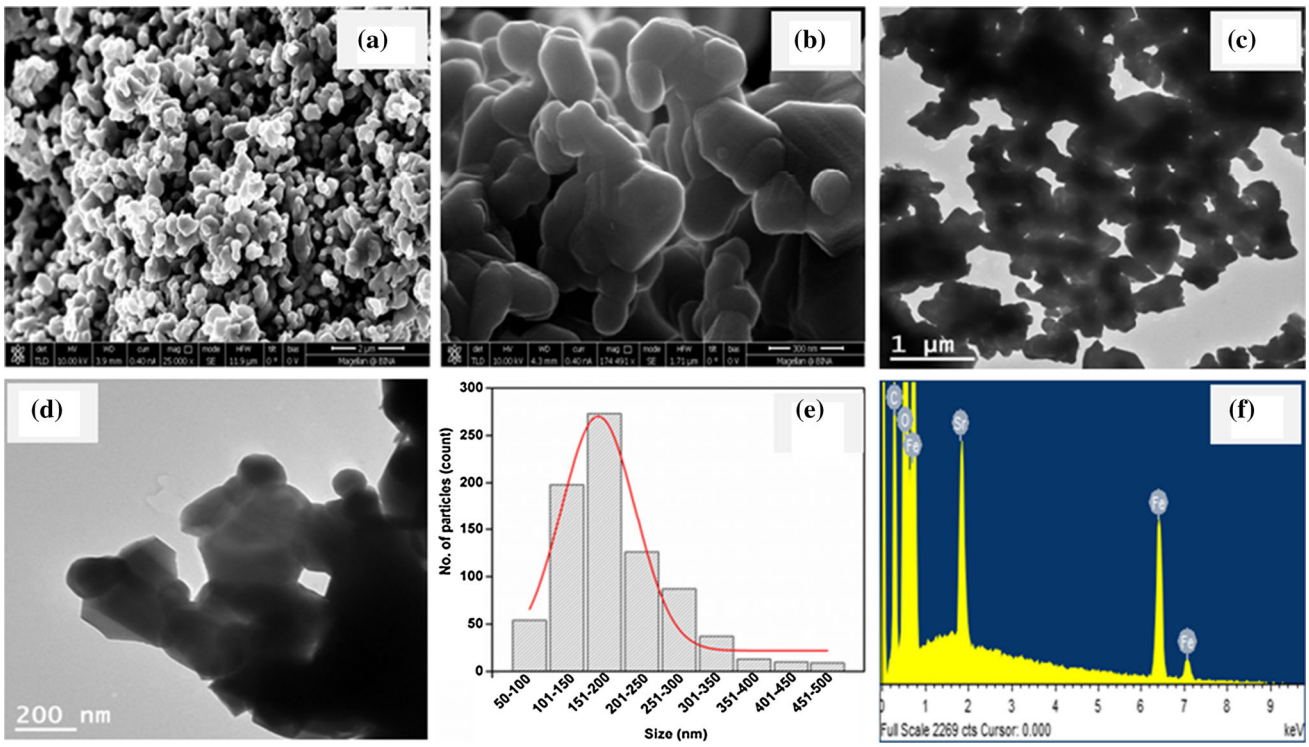

Fig. 4 Low and high magnification images of HRSEM (**a**–**b**), TEM images (**c**–**d**), histogram of particle size distribution (**e**), and EDX spectrum (**f**) of $SrFe_{12}O_{19}$ nanoparticles

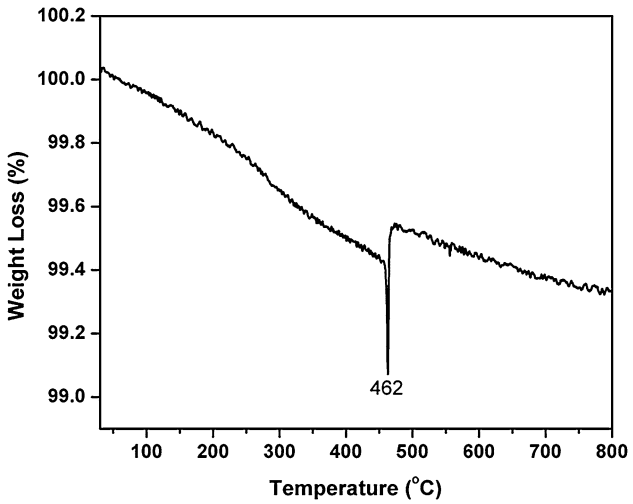

Fig. 5 TGA curve of $SrFe_{12}O_{19}$ nanoparticles with an external permanent magnet

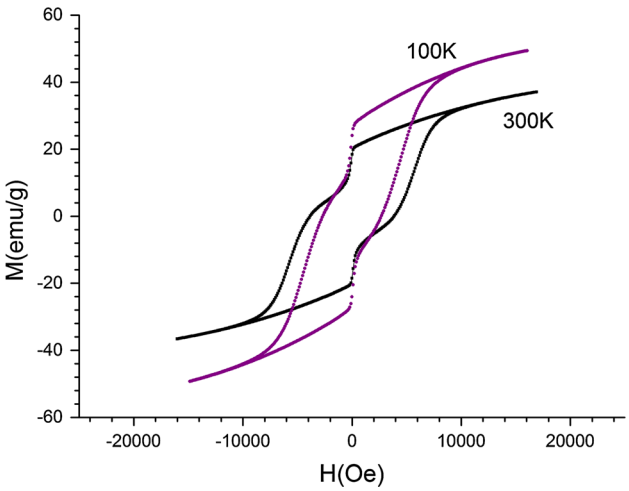

Fig. 6 Hysteresis loops of $SrFe_{12}O_{19}$ nanoparticles at 100 and 300 K

measured values of the saturation magnetization, M_s, the remnant magnetization, M_r, and the coercive field, H_c at 100 and 300 K, and compare the results to bulk data at room temperature published in the literature. While H_c measured in our sample are comparable to those reported for the bulk, the value of M_s is significantly lower, probably reflecting a size effect of the nanoparticles. Note that in Table 1 the M_s is taken to be the magnetization for the maximum field used. The data imply a slow increase at higher fields probably due to superparamagnetic contribution from the smaller particles.

In a sample of isolated magnetic particles, one expects to observe size effects when the particles size drops below a critical size, D_m, which can be estimated as [5, 37]

$$D_m = 9\sigma_w/2\pi M_s^2 \quad (3)$$

Table 1 Values of the saturation magnetization (M_s), the remnant magnetization (M_r), and the coercive field (H_c) in bulk and nanoparticles of $SrFe_{12}O_{19}$

	M_s (emu/g)	M_r (emu/g)	$H_c(Oe)$
$SrFe_{12}O_{19}$ nanoparticles (100 K)*	44	27	2600
$SrFe_{12}O_{19}$ nanoparticles (300 K)*	33	21	3800
$SrFe_{12}O_{19}$ nanoparticles (300 K)**	32	19	4600
$SrFe_{12}O_{19}$ nanoparticles (300 K)***	24.7	10.9	3500
$SrFe_{12}O_{19}$ Bulk (300 K)***	78.5	31	3500
$SrFe_{12}O_{19}$ Bulk (300 K)****	70.5	40	3004

* This work; ** Ref. [33]; *** Ref. [15];**** Ref. [36]

where $\sigma_w = (2k_bT_cK_1/a)^{0.5}$ is the domain wall energy, k_b is Boltzmann constant, K_1 the magnetocrystalline anisotropy and a is the lattice constant. Taking the bulk values $T_c = 723$ K [35], $a = 5.88 \times 10^{-8}$ cm from our XRD measurements, $M_s = 70.5\frac{\text{emu}}{\text{g}} = 374Oe$ [36], and $K_1 = 3.57 \times 10^6 \text{erg/cm}^3$ [5], one obtains $D_m \sim 350$ nm. As most of the particles in our sample are smaller than this value (see Fig. 4e) one may expect to see a superparamagnetic behavior of the sample. This is, of course, not the case because of the tendency of the particles to aggregate. Nevertheless, a signature of the magnetic behavior of the individual nano-particles can still be observed in the unusual behavior of the magnetic hysteresis loop (Fig. 6). This loop shows neither the superparamagnetic behavior expected for nanoparticles nor the hysteresis behavior expected for multi-domain particles. We propose that the measured loop is a superposition of the two, reflecting the fact that our sample consists of large aggregates and small isolated particles. As a way of illustration, we show in Fig. 7 a schematic behavior of the magnetization of nanoparticles (dotted curve, based on a Langevin function) and large particles of equal volume (dashed curve). Apparently, the solid curve that shows the superposition of the two contributions is similar to the measured magnetization curve shown in Fig. 6.

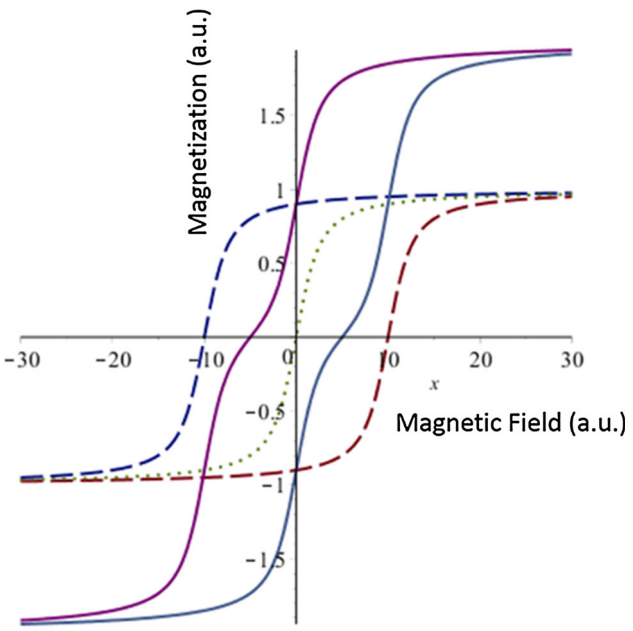

Fig. 7 Schematic behavior of the magnetization of nano-particles (*dotted curve*) and large particles of equal volume (*dashed curve*). The *solid curve* shows the superposition of the two contributions

Incidentally, the experimental ratio $M_r/M_s \sim 0.5$ (see Fig. 6) is consistent with the Stoner–Wohlfarth magnetization model [38] for randomly oriented identical magnetic particles. However, as apparent from Fig. 6, the magnetic behavior cannot be described by this model.

4 Summary and conclusions

M-type strontium hexaferrite ($SrFe_{12}O_{19}$) a hard magnetic nanopowder was successfully synthesized by a facile sonochemical strategy and subsequently calcination process. The obtained nanopowder was characterized by XRD, HRSEM, TEM, BET, TGA, and SQUID measurements. XRD observation showed that all the diffraction peaks of the obtained product were consistent with those of the single phase, hexagonal structure and P63/mmc (194) space group. The mean primary crystallite size (D) from the Scherrer's equation and lattice parameters (a, c) were calculated to be D = 44 nm, a = 0.5884 nm, and c = 2.3035 nm, respectively. From the low magnification HRSEM image, the diameter of the nanoparticles was between 50 and 500 nm. $SrFe_{12}O_{19}$ particles shown the roughly spherical-like morphology and the average particles size was 200 nm. This size according to our interpretation corresponds to an aggregate composed of 50 nm size particles. The atomic ratio of strontium (Sr^{2+}) to iron (Fe^{3+}) detected from the EDX spectrum was approximately 1:12. The BET measurement result of the specific surface area was 8.1 $m^2\ g^{-1}$. The Curie temperature (T_c) of the sample, deduced from TGA measurement under magnetic field was 462 °C. SQUID measurement revealed saturation magnetization significantly lower than that measured for a bulk sample, probably reflecting a size effect in the nanoparticles.

Acknowledgments P. Sivakumar thanks the Council for Higher Education, State of Israel for providing him the PBC postdoctoral fellowship. Prof. Yosef Yeshurun acknowledges a support from the Israel Science Foundation.

References

1. R.C. Pullar, Hexagonal ferrites: a review of the synthesis, properties and applications of hexaferrite ceramics. Prog. Mater Sci. **57**, 1191–1334 (2012)
2. J. Smit, H.P.J. Wijn, Ferrites, Philips' technical library, 1959
3. A. Vijayalakshmi, N.S. Gajbhiye, Magnetic properties of single-domain $SrFe_{12}O_{19}$ particles synthesized by citrate precursor technique. J. Appl. Phys. **83**, 400–406 (1998)
4. T.T.V. Nga, N.P. Duong, T.T. Loan, T.D. Hien, Key step in the synthesis of ultrafine strontium ferrite powders ($SrFe_{12}O_{19}$) by sol–gel method. J. Alloy. Compd. **610**, 630–634 (2014)
5. Z.F. Zi, Y.P. Sun, X.B. Zhu, Z.R. Yang, J.M. Dai, W.H. Song, Structural and magnetic properties of $SrFe_{12}O_{19}$ hexaferrite synthesized by a modified chemical co-precipitation method. J. Magn. Magn. Mater. **320**, 2746–2751 (2008)
6. A. Drmota, M. Drofenik, A. Znidarsic, Synthesis and characterization of nano-crystalline strontium hexaferrite using the co-precipitation and microemulsion methods with nitrate precursors. Ceram, Inter. **38**, 973–979 (2012)
7. O. Mohanta, Y.N. Singhbabu, S.K. Giri, D. Dadhich, N.N. Das, R.K. Sahu, Degradation of congo red pollutants using microwave derived $SrFe_{12}O_{19}$: an efficient magnetic photocatalyst under visible light. J. Alloy. Compd. **564**, 78–83 (2013)
8. Z. Wang, L. Zhong, J. Lv, H. Qian, Y. Zheng, Y. Fang, M. Jin, J. Xu, Microwave-assisted synthesis of $SrFe_{12}O_{19}$ hexaferrites. J. Magn. Magn. Mater. **322**, 2782–2785 (2010)
9. S.F. Wang, C. Zhang, G. Sun, B. Chen, W. Liu, X. Xiang, H. Wang, L. Fang, Q. Tian, Q. Ding, X. Zu, Effect of carbon and sintering temperature on the structural and magnetic properties of $SrFe_{12}O_{19}$ nanoparticles. J. Sol–Gel Sci. Technol. **73**, 371–378 (2015)
10. S.K. Chawla, P. Kaur, R.K. Mudsainiyan, S.S. Meena, S.M. Yusuf, Effect of fuel on the synthesis, structural, and magnetic properties of M-type hexagonal $SrFe_{12}O_{19}$ nanoparticles. J. Supercond. Nov. Magn. **28**, 1589–1599 (2015)
11. S.M. Mirkazemi, S. Alamolhoda, Z. Ghiami, Microstructure and magnetic properties of $SrFe_{12}O_{19}$ nano-sized powders prepared by sol–gel auto-combustion method with CTAB surfactant. J. Supercond. Nov. Magn. **28**, 1543–1549 (2015)
12. S.M. Mirkazemi, S. Alamolhoda, Z. Ghiami, Erratum to: microstructure and magnetic properties of $SrFe_{12}O_{19}$ nano-sized powders prepared by sol–gel auto-combustion method with CTAB surfactant. J. Supercond. Nov. Magn. **28**, 1551–1558 (2015)
13. H. Luo, B.K. Rai, S.R. Mishra, V.V. Nguyenb, J.P. Liu, Physical and magnetic properties of highly aluminum doped strontium ferrite nanoparticles prepared by auto-combustion route. J. Magn. Magn. Mater. **324**, 2602–2608 (2012)
14. Y.F. Xu, Y.Q. Ma, S.T. Xu, F.L. Zan, G.H. Zheng, Z.X. Dai, Effects of vacancy and exchange-coupling between grains on magnetic properties of $SrFe_{12}O_{19}$ and α-Fe_2O_3 composites. Mater. Res. Bull. **57**, 13–18 (2014)
15. M. Jean, V. Nachbaur, J. Bran, J.M. Le Breton, Synthesis and characterization of $SrFe_{12}O_{19}$ powder obtained by hydrothermal process. J. Alloy. Compd. **496**, 306–312 (2010)
16. A. Baykal, Solvothermal synthesis of pure $SrFe_{12}O_{19}$ hexaferrite nanoplatelets. J. Supercond. Nov. Magn. **27**, 877–880 (2014)
17. S. Shafiu, H. Sözeri, A. Baykal, Solvothermal synthesis of $SrFe_{12}O_{19}$ hexaferrites: without calcinations. J. Supercond. Nov. Magn. **27**, 1593–1598 (2014)
18. F.M. Gu, W.W. Pan, Q.F. Liu, J.B. Wang, Electrospun magnetic $SrFe_{12}O_{19}$ nanofibres with improved hard magnetism. J. Phys. D Appl. Phys. **46**, 445003–445009 (2013)
19. S.M. Masoudpanah, S.A.S. Ebrahimi, Influence of metal precursor on the synthesis and magnetic properties of nanocrystalline $SrFe_{12}O_{19}$ thin films. J. Magn. Magn. Mater. **343**, 276–280 (2013)
20. J.R. Liu, R.Y. Hong, W.G. Feng, D. Badami, Y.Q. Wang, Large-scale production of strontium ferrite by molten-salt-assisted coprecipitation. Powder Tech. **262**, 142–149 (2014)
21. L.A. Trusov, A.V. Vasiliev, M.R. Lukatskay, D.D. Zaytsev, M. Jansen, P.E. Kazin, Stable colloidal solutions of strontium hexaferrite hard magnetic nanoparticles. Chem. Commun. **50**, 14581–14584 (2014)
22. A. Javidan, S. Rafizadeh, S.M.H. Mashkani, Strontium ferrite nanoparticle study: thermal decomposition synthesis, characterization, and optical and magnetic properties. Mater. Sci. Semicond. Proc. **27**, 468–473 (2014)
23. E. Kiani, A.S.H. Rozatian, M.H. Yousefi, Synthesis and characterization of $SrFe_{12}O_{19}$ nanoparticles produced by a low-temperature solid-state reaction method. J. Mater. Sci.: Mater. Electron. **24**, 2485–2492 (2013)
24. V.G. Kostishyn, L.V. Panina, L.V. Kozhitov, A.V. Timofeev, A.N. Kovalev, Synthesis and multiferroic properties of M-type $SrFe_{12}O_{19}$ hexaferrite ceramics. J. Alloy. Compd. **645**, 297–300 (2015)
25. A.M.B. Miró, F.S.D. Jesús, C.A.C. Escobedo, S.D.D. Torre, R. Valenzuela, Synthesis of M-type $SrFe_{12}O_{19}$ by mechanosynthesis assisted by spark plasma sintering. J. Alloy. Compd. **643**, S226–S230 (2015)
26. G.H. An, T.Y. Hwang, Y.H. Choa, K. Shin, Synthesis of size-controlled SrFe12O19 using modified spray pyrolysis-calcination method and their magnetic properties. J. Electron. Mater. **43**, 3574–3581 (2014)
27. W. Lv, Q. Qiu, F. Wang, S. Wei, B. Liu, Z. Luo, Sonochemical synthesis of cobalt aluminate nanoparticles under various preparation parameters. Ultrason. Sonochem. **17**, 793–801 (2010)
28. G. Applerot, J. Lellouche, A. Lipovsky, Y. Nitzan, R. Lubart, A. Gedanken, E. Banin, Understanding the antibacterial mechanism of CuO nanoparticles: revealing the route of induced oxidative stress. Small **8**, 3326–3337 (2012)
29. Q. Li, H. Li, V.G. Pol, I. Bruckental, Y. Koltypin, J.C. Moreno, I. Nowike, A. Gedanken, Sonochemical synthesis, structural and magnetic properties of air-stable Fe/Co alloy nanoparticles. New J. Chem. **27**, 1194–1199 (2003)
30. E. Malka, I. Perelshtein, A. Lipovsky, Y. Shalom, L. Naparstek, N. Perkas, T. Patick, R. Lubart, Y. Nitzan, E. Banin, A. Gedanken, Eradication of multi-drug resistant bacteria by a novel Zn-doped CuO nanocomposite. Small **23**, 4069–4076 (2013)
31. K. Vinodgopal, B. Neppolian, I.V. Lightcap, F. Grieser, M. Ashokkumar, P.V. Kamat, Sonolytic design of graphene-Au nanocomposites. Simultaneous and sequential reduction of graphene oxide and Au(III). J. Phys. Chem. Lett. **1**, 1987–1993 (2010)
32. B. Li, Y. Xie, J. Huang, Y. Liu, Y. Qian, A novel method for the preparation of III–V semiconductors: sonochemical synthesis of InP nanocrystals. Ultrason. Sonochem. **8**, 331–334 (2001)
33. M. Sivakumar, A. Gedanken, W. Zhong, Y.W. Du, D. Bhattacharya, Y. Yeshurun, I. Felner, Nanophase formation of strontium hexaferrite fine powder by the sonochemical method using $Fe(CO)_5$. J. Magn. Magn. Mater. **268**, 95–104 (2004)
34. I. Perelshtein, N. Perkas, Sh Magdassi, T. Zioni, M. Royz, Z. Maor, A. Gedanken, Ultrasound-assisted dispersion of $SrFe_{12}O_{19}$

nanoparticles in organic solvents and the use of the dispersion as magnetic cosmetics. J. Nanopart. Res. **10**, 191–195 (2008)
35. B.D. Cullity, C.D. Grahm, *Introduction to Magnetic Materials*, 2nd edn. (Wiley-IEEE Press, Piscataway, NJ, 2009), pp. 487–488
36. A. Xia, C. Zuo, L. Zhang, C. Cao, Y. Deng, W. Xu, M. Xie, S. Ran, C. Jin, X. Liu, Magnetic properties, exchange coupling and novel stripe domains in bulk $SrFe_{12}O_{19}$/(Ni, Zn)Fe_2O_4 composites. J. Phys. D Appl. Phys. **47**, 415004–415014 (2014)
37. J. Smit, H.P.J. Wijn, *Les Ferrites* (Dunod, Paris, 1961)
38. E.C. Stoner, E.P. Wohlfarth, A mechanism of magnetic hysteresis in heterogeneous alloys. Philos. Trans. R. Soc. Lond. A **240**, 599–642 (1948)